Gas and Water Flood Gravity Drainage in Viscous Oil Field Developments

Nicola Sargent, David Element, Stephen Goodyear and Jane Johnston

AEA Technology, Winfrith, Dorchester, Dorset DT2 8DH, UK

ABSTRACT

Water flooding and gas injection into a primary gas cap, where this exists, provide alternative strategies for the development of viscous oil fields. Most UKCS viscous oil reservoirs are of excellent quality, comprised of unconsolidated sands with high horizontal and vertical permeability. Gas injection may give lower effective residual oil saturations due to the much greater density contrast between oil and gas compared to that between water and oil. A comparison of gas and water gravity drainage over a range of viscosities allows the potential benefits from gas injection and water flooding to be assessed.

Measurements of gas/oil relative permeabilities are typically made under viscous dominated flooding conditions, which are unrepresentative of gravity drainage conditions in the field, and without the benefit of in-situ saturation monitoring which is essential to remove laboratory artefacts arising from capillary end effects. To address these issues we performed a series of both gas/oil and water/oil gravity drainage experiments in three sandpacks, with permeabilities representative of UKCS viscous oil fields. Oils with viscosities varying from 2 cp to 210 cp have been used. Oil drainage was measured using in-situ saturation monitoring. The in-situ saturation data has been analysed to provide fractional flow and relative permeability data.

For the gas gravity drainage, oil relative permeabilities were found to be independent of viscosity and significantly higher than data in consolidated sandstone. Calculation of effective residual saturations at a range of reservoir viscosities and displacement rates, show that under appropriate conditions, very low oil saturations can be achieved.

Similarly, fractional flow curves derived from the water flood experiments did not exhibit any significant dependence on oil viscosity. A comparison of oil recoveries for waterflooding and gas injection shows gas injection can be preferable for high viscosity oils – particularly in more permeable reservoirs.

INTRODUCTION

Gas injection into a primary gas cap, where this exists, may provide an alternative strategy to water flooding for UKCS high permeability viscous oil fields, giving lower effective residual oil saturations (because of the much greater density contrast between oil and gas compared to that between water and oil). A series of gas gravity drainage floods has been performed in three separate sandpacks, using oils with viscosity ranging from 2.5 to 210 cp. Data from these experiments was used to deduce oil relative permeability, and the effective residual oil saturation to gas flooding over a wide range of viscosities. The sandpacks were subsequently employed in a series of water floods experiments at typical field rates, providing complementary data to the gas injection studies, so that the effective residual oil saturations to gas and water flooding can be assessed directly.

Two-phase in-situ saturations were measured using a single energy γ-attenuation technique. In-situ monitoring is essential to enable relative permeabilities to be calculated without experimental artefacts such as capillary end effects.

LABORATORY PROCEDURES

Preparation of Sandpacks

Three sandpacks were constructed using glass columns 2.5 cm in diameter, with pack lengths of approximately 70 cm. Fine filters separate the sand from the end caps to prevent sand grains entering the fluid lines. The sand was selected to give pack permeabilities of approximately 5 Darcy at 100% brine saturation, representative of UKCS viscous oil fields. The porosity of each pack was 47%. As the in-situ monitoring system requires 100% gas calibration, the column was dry-packed.

Fluids

Chesil seawater was selected as the brine phase. Kathon biocide was added to the brine at 5 ppm as the flood duration extended over several months. Nitrogen was used in the gas injection experiments.

Castrol's Magna lubricating oils were selected for the experiments due to their purity and wide viscosity range. The oil compositions used in the floods are given in Table 1. The Magna oils are highly refined straight mineral oils. Iodododecane was used to increase the γ-attenuation of the oil phase and optimise phase analysis. Exposure of the doped oils to light was minimised since iodododecane is photosensitive [1]. All three oils were checked to ensure that they spread on the brine. Attenuation scans were conducted on doped oil samples throughout the experiments in order to assess any degradation with time.

Table 1. Composition and Characteristics of Test Oils

				Gas Injection Experiments		Waterflood Experiments	
Sandpack	Ratio of component			Viscosity at 22°C (cp)	Density at 22°C (g/cc)	Viscosity at 22°C (cp)	Density at 22°C (g/cc)
	Magna 320	Magna 2	Iododo-decane				
1	4	-	1	208	0.944	210	0.944
2	-	4	1	2.7	0.877	2.5	0.877
3	2.4	1.6	1	23.5	0.917	21.7	0.916

Measurement of In-situ Saturations

The fluid saturations in the sandpacks were monitored during floods by gamma attenuation, using collimated Americium-241 sources and CsI scintillation detectors. The gamma-attenuation method can only be used to measure two phases. However, it can be used in three phase floods, provided one of the phases is immobile. Calibrations are required at 100% saturation of the fluids to be used in the experiment for each sandpack. No water was produced during the gas injection phase of the floods and agreement between effluent and in-situ mass balances was good. 100% gas calibrations were obtained for the dry sandpacks and 100% water calibrations when the sandpacks had been vacuum saturated with degassed brine. The 100% oil calibrations were measured at the end of the gas and water floods after mild solvent cleaning and flooding to 100% oil saturation with the same oil as had been used in the experiments.

The movement of the source/detector assembly and the collection of the counts was computer controlled, enabling automated scanning. The columns were scanned at 0.5 cm intervals along the complete length of the column. At the end of each scan a datum reference reading was taken on an aluminium bar positioned below the sandpacks. The datum counts were compared with an average reading taken on the bar at the start of the experiments so that a correction factor could be calculated to account for any changes in the characteristics of the electronics. Individual data points were then corrected by this factor.

The rig was contained in an air-conditioned laboratory maintained at a temperature of 22+/-0.5^{o}C.

CORE FLOODING SEQUENCE

Flood to Connate Water

Once 100% brine calibrations had been obtained, all the sandpacks were flooded to connate brine with the 208 cp oil (doped with 20% iodododecane). The same oil was used for all the sandpacks to enable a direct comparison to be made between the experiments without large differences in the magnitude of the connate brine saturations. Fluids were recirculated via a volume separator so that a mass balance determination of connate brine saturation could be made. The floods were stopped when there was no further brine production in the recirculating reservoir, the oil distribution (as indicated via attenuation scans) was constant, and reproducible permeabilities had been established.

Ageing with Stock Tank Oil

At the end of the connate water flood the heavy oil was displaced with kerosene, and the kerosene was then displaced with stock tank crude oil. The kerosene was used as a buffer to avoid potential asphaltene deposition on mixing heavy oil directly with stock tank oil. The core was aged for a period of 20 days. At the end of the ageing period the stock tank oil was displaced by kerosene and the kerosene was then displaced with the doped refined oil until the attenuation scans were constant.

Gravity Stable Gas Flood

The flow circuit used for the secondary nitrogen injection is illustrated in Figure 1. Nitrogen was supplied to the top of the sandpack at approximately 4 bar(g) via a partially filled brine column which saturated the gas phase with water vapour.

The outlet of the sandpack was connected to a calibrated separator which was initially filled with demineralised water. Water was extracted from the bottom of the separator at a constant rate whilst produced fluids entered the top of the separator. The fluids were extracted at a nominal rate of 0.2 ml/hr from Sandpacks 1 and 3 and 2 ml/hr from Sandpack 2. A higher fluid extraction rate was selected for the gas injection experiment in sandpack 2 in order to increase the amount of drainage observed behind the gas front – thus allowing relative permeabilities to be calculated over a meaningful range of saturations. The volumes of the produced phases were measured by monitoring the levels of the phase interfaces in the separator.

Flood to Connate Water

In preparation for the waterflood experiments, each sandpack was flooded with toluene from 100% oil saturation until the effluent was "clean". The toluene was then displaced with methanol. The sandpacks were then flooded with degassed Chesil brine until the effluent was pure brine. New 100% brine γ-attenuation calibrations were obtained, prior to flooding all of the sandpacks to connate brine with the 210 cp oil (doped with 20% iodododecane).

Ageing with Stock Tank Oil

At the end of the connate water flood the heavy oil was displaced with kerosene, and the kerosene was then displaced with stock tank crude oil. The core was aged for a period of 10 days (noting that the sandpacks had been aged for the initial gas injection experiments, and subsequently mildly cleaned).

At the end of the ageing period the stock tank oil was displaced by kerosene. However, at the end of the kerosene flood stock tank oil was still visible at the ends of the sandpacks indicating a less efficient sweep or a different character in these end zones.

The kerosene was displaced from each sandpack using the three doped refined oils, until the attenuation scans were constant and permeability established.

Water Flood

The flow circuit for waterflooding is similar to that in Figure 1, except that water was flooded vertically upwards through the sandpacks and fluids were recirculated via a volume separator. The flow rate for sandpack 1, the most viscous oil, was calculated to give a frontal advance rate typical of reservoir rates in basal drive waterfloods. The flow rates for the other sandpacks were then obtained by a ratio of the rate to the density difference of the brine and the oil to be used.

After water breakthrough, saturation data was collected during periods of shut-in, and of flooding at increased rates. It is beyond the scope of this paper to discuss those additional waterflood measurements.

RESULTS

The measured in-situ saturation profiles for the three gas drainage experiments are plotted in Figures 2, 3 and 4. The spatial distribution of the initial brine saturation, prior to the gas injection, is reasonably constant across the centre of each of the sandpacks. Saturation data during waterflooding are plotted in Figures 5, 6 and 7.

Table 2 summarises breakthrough characteristics for the experiments. With the low viscosity oil the recovery was high, and similar for both gas injection and waterflooding. Anticipated residual oil saturations (extrapolating to very large flooding volumes) were also similar for the two floods. Oil recovery was also high for the gas injection with 23.5 cp oil. At this viscosity (and for the experimental conditions) gas injection represents a more attractive development strategy than waterflooding. Recovery is less for the more viscous oils, with gas injection still proving to be slightly more favourable than waterflooding.

Table 2. Gas Injection and Waterflood Experiments

Sandpack	Viscosity (cp)		Swc (%)		Flow rate (ml/hr)		Breakthrough PV		Mean So at breakthrough	
	gas	water	gas	water	gas	water	gas	water	gas	water
2	2.7	2.5	12	11	2.0	0.46	0.75	0.67	0.21	0.21
3	23.5	21.7	11	10	0.19	0.35	0.71	0.52	0.19	0.38
1	208	210	9	8	0.2	0.26	0.34	0.30	0.56	0.61

For waterflooding, the breakthrough volumes and saturations are based on the time water reached the pack outlet. In each pack end effects were observed to delay water breakthrough after the front had reached the end region of the pack.

Slight differences in oil viscosities tabulated above are due to the fluids being mixed at different times.

2.7 cp oil (Sandpack 2)

The gas gravity displacement is very efficient, with very little evidence of local hold-up of oil at the end of the flood. Following gas injection, the profiles show high oil saturations near the inlet throughout the gas flood (thought to be an artefact associated with the injection of the stock oil) and some hold-up of oil near the outlet as a result of a capillary pressure end effect.

During waterflooding the shock front was well defined, indicating a stable flood front. The in-situ saturation measurements showed inlet and outlet core artefacts. These were possibly caused by the presence of stock tank oil at both ends of the sandpack - since stock tank oil was visible prior to waterflooding. The in-situ saturation profiles indicated that oil was held up at the core outlet, so the water breakthrough time estimated from mass balance was artificially delayed. The breakthrough characteristics quoted in Table 2 are based on in-situ measurements and avoid the errors caused by oil hold-up.

23.5 cp oil (Sandpack 3)

At the end of gas injection, as in sandpack 2, the profiles show high oil saturations near the inlet and some evidence for a capillary pressure end effect. The gas gravity displacement is efficient, with little evidence of local hold-up of oil.

The waterflood saturation distributions indicate a stable water front, with a well defined shock front. As with sandpack 2, hold-up of oil at the core outlet affects the time at which water breaks through to the end of the pack.

208 cp oil (Sandpack 1)

Following gas injection, as in sandpacks 2 and 3, the gas/oil saturation profiles show an inlet artefact and some evidence for a capillary pressure end effect. Early in the flood the saturation profiles in the central regions of the core show significant local variations in saturation, although at later times these become less pronounced as oil continues to drain under the action of gravity.

The waterflood saturation profiles provide evidence of inlet and outlet core artefacts. This flood was not gravity stable. Although the in-situ saturation profiles indicated that oil was held up at the core outlet, the breakthrough characteristics quoted in Table 2 are similar to those determined by mass balance.

Each of the three waterflood experiments exhibited the same interesting characteristics after water had reached the outlet region of the pack. After that time, the oil saturations in the bulk of the pack dropped more rapidly than before, while in the final 5-10 cm of each of the packs the oil saturation remained at a very high value.

ANALYSIS OF IN-SITU SATURATION DATA FOR GAS/OIL RELATIVE PERMEABILITIES & WATER/OIL FRACTIONAL FLOWS

Theoretical Basis for Analysis Technique

The relative permeability can be computed from saturation data in a gravity dominated experiment using equation (1) (assuming that capillary pressure and viscous pressure drops can be neglected). V_o is the volume of oil upstream of depth *z*, at time *t*.

$$k_{ro}(z,t) = -\frac{m_o}{K(z)(r_o - r_g)gA} \cdot \frac{\partial}{\partial t} V_o(z,t), \qquad V_o(z,t) = A\int_0^z f S_o(z,t)dz, \tag{1}$$

Solving equation (1) requires some smoothing of the measured data. Reference [2] presents a variety of different smoothing methods. In this study, *variable time point t^{-b} (Buckley-Leverett) smoothing* has been employed, although all relative permeability calculations have been checked using the *variable time point e^{-bt} (exponential) smoothing*.

Equation (1) cannot be used for waterflood experiments, since viscous pressure drops are not negligible. However, the time-derivative of V_o gives a measure of local oil flow rate – which can be combined with the total flow rate to give fractional flow. Relative permeability and fractional flows were not calculated in regions influenced by end effects.

Permeability Distribution

Calculation of relative permeabilities using (1) requires local permeability values. Previous studies suggested that permeability could be different at the ends of the pack as a result of the packing procedure and the injection of stock tank oil. The pressure drop was monitored in each sandpack during the flood to connate water (displacing brine with 208 cp oil) and also when displacing kerosene with the Magna oils. As these are piston-like displacements (expect for displacing kerosene with the low viscosity 2.7 cp oil in sandpack 2), the local permeability at the oil front may be readily calculated using :

$$\frac{d(\Delta p/Q)}{dW} = \frac{1}{f\Delta SA^2}\left(\frac{m_D}{k_D(W/(f\Delta SA))} - \frac{m_i}{k_i(W/(f\Delta SA))}\right), \tag{2}$$

where $k_D(z)$ and $k_i(z)$ are the permeabilities to the displacing and in-place fluid respectively.

The noise in the pressure data meant that useful permeability data could only be derived by relatively coarse spatial-averaging, and so it was not possible to correlate permeability with the local porosity. However, an average permeability was determined in the central region excluded the low-permeability regions at the end of the packs (Table 3)

Table 3: Summary of Brine Permeability Data – for Gas Injection Experiments

	Central region permeabilities from viscous oil floods		Pack average permeabilities from total pressure drop	
	Before Ageing (md)	After Ageing (md)	Before Ageing (md)	After Ageing (md)
Sandpack 1	3,850	800	3,000	270
Sandpack 2	4,000	-	2,600	150
Sandpack 3	no data available	1,000	2,020	190

As Table 3 shows, the effect of ageing with crude oil is to reduce the permeability in the central region of each sandpack by a factor of approximately 4-5. Based on the analysis of permeability in the central region of each core, the average permeability value after ageing for the gas injection experiments was taken to be 900 md for each sandpack.

After flooding to 100% brine prior to the waterflooding experiment, the average brine permeabilities were found to be similar to those tabulated above. Absolute permeability values were estimated from pressure drop data while displacing kerosene with the doped Magna oils in packs 1 and 3. This displacement data confirms that absolute permeabilities are in the range 750-1700 md. A value of 1350 md

has been adopted to represent the absolute permeability value, *k*, for the waterflood experiments in all three packs away from the end regions. Overall pack permeability was determined from pressure drop during oil flow at connate brine saturation. This gave a permeability considerably lower than 1350 md, since the *average* pack permeability is likely to have been dominated by low permeabilities at the ends.

Sensitivity studies have been conducted for all of the calculations presented in this report, but the effect of absolute permeability on the shape of the water/oil fractional flow curves is small for all three packs.

Gas/Oil Relative Permeability Calculations

Relative permeabilities were calculated from the saturation data, except for positions near the ends of the sandpack since the inlet and outlet regions of the packs had much lower permeability, and towards the bottom of the pack capillary pressure effects are significant.

Relative permeabilities for the 208 cp oil (Sandpack 1) are shown in Figure 8. Data is grouped according to the depth at which each measurement was made. Although there is some scatter, the relative permeability values are clustered around an obvious trend. Oil saturation values range from 0.16 to 0.70 for this pack (the gravity dominated floods in the other two packs employed lower viscosity oils and therefore lower oil saturation values were attained).

The data shows a scatter of approximately a factor of 6 between the highest and lowest relative permeabilities for a given saturation. This scatter may reflect the fact that an average oil permeability is being used to calculate the relative permeabilities. Local changes in permeability will be reflected in artificially low relative permeabilities in low permeability zones, and artificially high relative permeabilities in high permeability zones. In this case, the local permeability would be expected to correlate with the local porosity, for which there is a direct measure from the 100% gas calibration scan in each sandpack. Attempts were made to reduce the scatter in the relative permeability data for all three sandpacks using a simple correlation linking porosity and the local permeability. This was not successful, except at a few isolated positions with relatively very low porosity. In the section on simulation of the corefloods it will be shown that in the presence of capillary pressure, the relative permeability computed at a particular depth station is not only sensitive to the local permeability, but also to the permeability in the neighbourhood of the spatial position at which it is calculated.

Since an average sandpack permeability has been assumed in the computation of relative permeabilities, the relative permeability values plotted in Figure 8 should really be considered as “effective relative permeabilities” based on the assumption of the sandpack having permeability of 900 md.

The relative permeabilities calculated from the saturation profiles for all three oils are compared in Figure 9. In the lower viscosity experiments, regions of lower computed relative permeability values were noted. The pack depths corresponding to those regions were shown to correspond to pack locations at which the porosity was significantly lower than elsewhere, and so are likely to correspond to a lower permeability at these positions compared to the core average.

Figure 9 clearly shows that, in spite of the different oil viscosities employed in each flood, the relative permeabilities are all clumped around a single trend-line. The data over the combined saturation range has been fitted to a standard Corey relative permeability equation:

$$k_{ro} = K_{ro}^{o}\left(\frac{S_o - S_{org}}{1 - S_{wc} - S_{org}}\right)^{n} : regression \rightarrow \quad k_{ro} = 3.55\left(\frac{S_o - 0.035}{1 - S_{wc} - 0.035}\right)^{2.85}, \tag{3}$$

where the average connate water saturation, S_{wc}, for all three sandpacks is 0.086.

The sandpack oil relative permeabilities have also been compared with relative permeabilities determined in previous studies using Clashach cores. Figure 10 includes the results of experiments in water-wet and intermediate wet Clashach sandstone [3]. Although the relative permeabilities were very similar for the different Clashach cores (from which it was concluded [3] that the change in rock wettability affected absolute permeability rather than oil relative permeability), the relative permeabilities computed for the three sandpacks are significantly higher. This would indicates that the very different pore structure of consolidated Clashach core and a sandpack affects both absolute permeability and oil relative permeability.

Water/Oil Fractional Flow Calculations

In-situ waterflood saturation data has been smoothed analytically, leading to the calculation of fractional flow data. The fractional flow is related to the relative permeabilities according to the equation:

$$f_w(S_w) = \frac{1-G}{1+\frac{m_w}{m_o}\frac{k_{ro}}{k_{rw}}}, \quad G(S_w) = \frac{k.k_{ro}.A.\Delta r}{q.m_o}. \tag{4}$$

At higher water saturations, fractional flow data may be expected to lie on the curve defined by equation 4. At lower water saturations the data lies on the straight line representing the tangent from the initial water saturation to equation 4. The tangent line indicates a shock front.

Fractional flow data from all three waterfloods are plotted in Figure 11. Taken as a set, the three packs cover a range of mobilities. If a permeability of 1350 md is assumed, then $G(S_w)$ is just $0.033k_{ro}$ for sandpack 1 (the frontal advance of water was not gravity stable in this pack), but $2.95k_{ro}$ for sandpack 2.

Performing a regression analysis for the combined set of fractional flow data from Figure 11 gives the following expression (assuming that relative permeabilities may be described by Corey equations):

$$All\,sandpacks: f_w(S_w) = \frac{1-G}{1+1.0\frac{m_w}{m_o}\frac{(1-S_w-0.08)^{2.4}}{(S_w-0.08)^{3.2}}}. \tag{5}$$

Figure 11 compares this equation to the experimental water fractional flow data, showing good agreement for packs 1 and 2, although the experimental water fractional flow values for pack 3 lie slightly above the line representing equation 5. Regression analysis reveals a range of solutions similar to equation 5 which could all be considered to be equally good matches to the experimental fractional flow data.

Sensitivity studies have been conducted for the waterflood fractional flow calculations, demonstrating that the effect on the shape of the fractional flow curve of uncertainties in the absolute permeability value, *K*, is small for all three packs.

The fact that data from the three sandpacks can be represented by a single equation suggests that that the oil and water relative permeabilities are probably similar for all three sandpacks. If this is the case, relative permeability is not exhibiting any strong sensitivity to oil viscosity. The relative permeabilities for all packs may be represented by the following equations:

$$k_{ro}(S_w) = K_{ro}^{o}(1-S_w-0.08)^{2.4}, \quad k_{rw}(S_w) = K_{rw}^{0}(S_w-0.08)^{3.2}. \tag{6}$$

It is possible to estimate fractional flow by analysing saturation profiles measured in the waterflood experiments, and applying the familiar Buckley Leverett theory. This analysis technique gives rise to fractional flow curves consistent with those plotted in Figure 11. The main advantage of determining fractional flow data from the time derivative of smoothed oil volume data is that it indicates how fractional flow changes with both position and time, and therefore makes it possible to eliminate end effects.

SIMULATIONS OF GRAVITY DRAINAGE

Using the black oil option in *tech*SIM, a number of gas/oil gravity drainage experiments have been simulated, with the aim of understanding the temporary, local hold-up of oil observed in the saturation measurements made using 208 cp oil. The oil saturation profiles computed in simulations without capillary pressure exhibit “hold-up” of oil wherever permeability is lower than the average. The effect of non-zero capillary pressure is to reduce the oil saturation hold-up and also to raise the hold-up upstream of the tight zone. This smoothing of the oil saturation profile can be explained mathematically by differentiating the expression for the capillary pressure expected when equilibrium is reached at the end of gas/oil gravity drainage:

$$p_c(S_o(z)) = (L - z)g\Delta r, \quad \therefore g.\Delta r = \frac{d}{dz} p_c(S_o(z)) = \frac{dp_c}{dS_o} \frac{\P S_o}{\P z}. \tag{7}$$

The greater the slope dp_c/dS_o , the smaller any local fluctuations in S_o will be.

With non-zero capillary pressure the computed relative permeability values are not only reduced at the tight permeability zones, but also at depth stations close to these tight zones. The scatter of relative permeability datum points observed in the analysis of experimental data is caused not only by permeability heterogeneity, but also by capillary pressures. Even if an accurate permeability distribution were available for a sandpack, it would not be possible to remove scatter by scaling computed relative permeability values according to local permeability.

Figure 12 shows the oil saturations computed for a heterogeneous pack with local permeability ranging from 250 to 1931 md. The permeability profile (and other simulation parameters) were designed to give computed oil saturations similar to those observed in the gravity drainage experiments using the 208 cp oil. The mean permeability is 900 md, as in the actual sandpack. The simulation includes capillary pressure (without capillary pressure the degree of "noise" in the oil saturations would be higher than in Figure 12).

Most of the relative permeability values computed from simulated saturation profiles lie slightly *above* the relative permeability curve defined in simulator input, because most of the local permeability values are *higher* than the mean value of 900 md. The mean permeability reflects the *harmonic average* of local permeability values. The *arithmetic mean* of local permeability values is 1117 md, so that for most of the depth stations in the simulated pack, the local permeability is underestimated, leading to a computed relative permeability value which is higher than the average. Because of the difference between mean permeability and the arithmetic mean of local permeability values, relative permeabilities computed from analysis of oil saturations in a gas/oil gravity drainage represent *effective relative permeabilities*. (However, in these simulated gas/oil gravity drainage experiments these are very close to the actual relative permeabilities).

COMPARISON OF WATER FLOODING AND GAS INJECTION

One–dimensional Buckley Leverett calculations have been performed using the relative permeability curves, to assess the local recovery efficiency that might be expected in vertical gas and water displacements for typical reservoir conditions (in regions of the field not affected by coning or significant capillary pressure effects). The oil-gas and water-gas density difference was taken as 800 and 100 kg/m^3 respectively.

For vertical permeabilities of 1 and 5 Darcy, gas injection breakthrough recoveries are plotted in Figure 13. In the 5 Darcy case, with oil viscosities below ~100 cp the microscopic sweep is gravity dominated for displacement rates of ~10 ft/month and below. Note that the velocities represented on the Buckley-Leverett plots are *interstitial velocities*, given by the Darcy velocity divided by porosity. Under appropriate conditions, effective residual oil saturations of ~10% may be obtained for oils of 100 cp viscosity.

Breakthrough recoveries have been compared in waterflood and gas injection calculations, using the relative permeabilities defined in equations (3) and (6) – see, for example, Figure 14. In a lower permeability (1 Darcy) reservoir, gas injection gives better local recovery than waterflooding for oil viscosities in the range 10-100 cp. In higher permeability (5 Darcy) reservoir flooded at the same rate, gas injection represents a better option than waterflooding for oil viscosities in the range ~30-1000 cp. In practice a decision between water and gas flooding will need to take into account the overall displacement stability, water and gas handling issues, and local sweep efficiency.

CONCLUSIONS

In-situ saturation data has been collected for a series of gas injection and waterflood experiments, using oils covering the viscosity range 2 to 200 cp.

From the gas/oil in-situ saturation data, oil relative permeabilities have been calculated for the three sandpacks. The relative permeabilities lie on the same curve, independent of oil viscosity. Comparison of the sandpack relative permeabilities with data obtained from consolidated Clashach sandstone, shows that the relative permeabilities in the sandpacks are approximately a factor of 300 higher over the saturation range considered. Gravity drainage in high permeability unconsolidated reservoirs, even with viscous oils, is therefore potentially a very efficient displacement technique.

Fractional flow data has been derived from the waterflood experiments. A single expression for fractional flow is suitable for characterising data from all three packs, suggesting that the oil and water relative permeabilities are not strongly dependent on oil viscosity.

One dimensional solutions for vertical displacement of oil by both gas and water have been constructed, determining the effective local residual oil saturation at breakthrough for viscosities from 1 cp to 1000 cp. Various frontal advance rates were considered (including typical reservoir rates) for vertical permeabilities of 1 and 5 Darcy. Under appropriate conditions, effective residual oil saturations of ~10% may be obtained with gravity drainage for oils of 100 cp viscosity. In higher permeability (5 Darcy) reservoirs, gas injection can represent a better option than waterflooding for oil viscosities in the range ~30-1000 cp. In a 1 Darcy reservoir, gas injection gives a higher recovery at breakthrough for oil viscosities in the range 10-100 cp.

NOMENCLATURE

A	pack cross-sectional area
F_w	water fractional flow
G	gravity term in fractional flow equation
K	absolute permeability
$k_D(z)$	permeability of displacing phase at position z from core inlet (equation 2)
$k_i(z)$	Permeability of phase initially present at position z from core inlet (equation 2)
K_{ro}^0	Corey coefficient
k_{rg}	gas relative permeability
k_{ro}	oil relative permeability
k_{rw}	water relative permeability
L	pack length
N	Corey exponent
p_c	capillary pressure
Q	flood flow rate
S_g	gas saturation
S_o	oil saturation
S_{org}	residual oil saturation to gas flooding
S_{wc}	connate water saturation
S_w	water saturation
t	time
V_o	volume of oil upstream of depth z, at time t (see equation 1)
W	total volume of injected fluid
z	Distance from sandpack inlet
Dp	pressure drop
Dr	Density difference
m_D	viscosity of displacing phase in local permeability calculation (equation 2)
m_i	viscosity of phase initially present in local permeability calculation (equation 2)
m_g	gas viscosity
m_o	oil viscosity
m_w	water viscosity
f	porosity

ACKNOWLEDGEMENT

This work was supported by the UK Department of Trade and Industry as part of its HARP studies at AEA Technology. The DTI's permission to publish is gratefully acknowledged.

REFERENCES

1. Aldrich Catalogue Handbook of Fine Chemicals 1996-7, p882
2. Goodyear, S.G., Jones, P.I.R., "Relative Permeabilities for Gravity Stabilised Gas Injection", *7th European Symposium on Improved Oil Recovery*, Moscow, Russia October 1993
3. Naylor, P., Sargent, N.C., Crosbie, A.J., Tilsed, A.P., Goodyear, S.G., "Gravity Drainage During Gas Injection", *Petroleum Geoscience*, Vol. 2, 1996, pp.69-74.

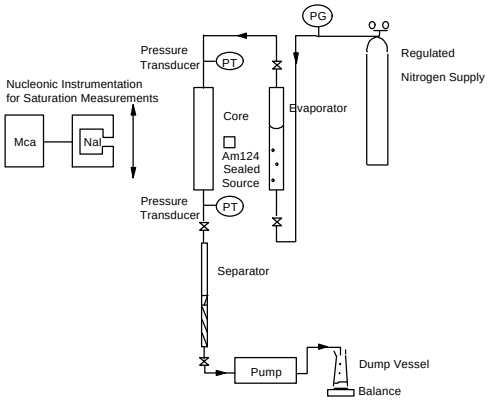

Figure 1: Schematic Diagram of Gas Injection Flow Circuit

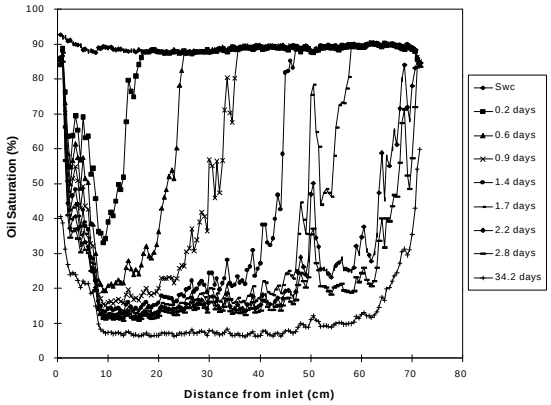

Figure 2: Oil Saturation Profiles for Gas Gravity Drainage of 2.7 cp Oil (Sandpack 2)

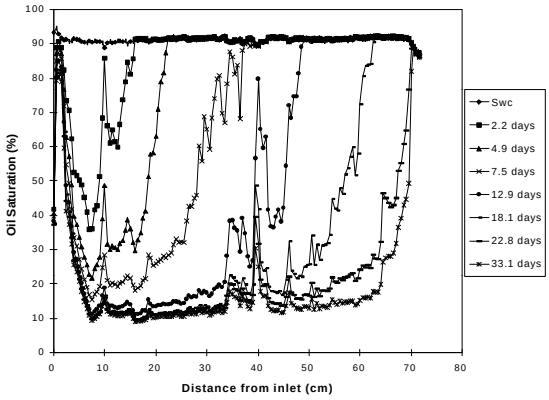

Figure 3: Oil Saturation Profiles for Gas Gravity Drainage of 23.5 cp Oil (Sandpack 3)

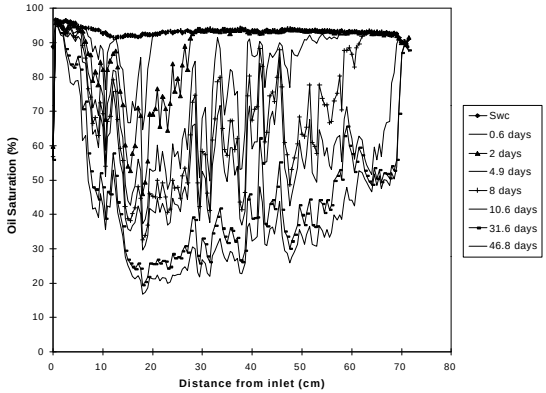

Figure 4: Oil Saturation Profiles for Gas Gravity Drainage of 208 cp Oil (Sandpack 1)

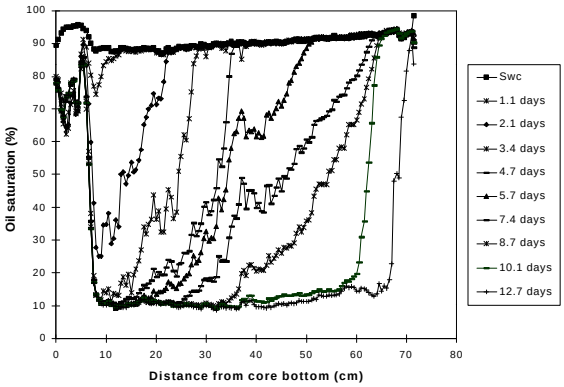

Figure 5: Oil Saturation Profiles for Waterflood of 2.5 cp Oil (Sandpack 2)

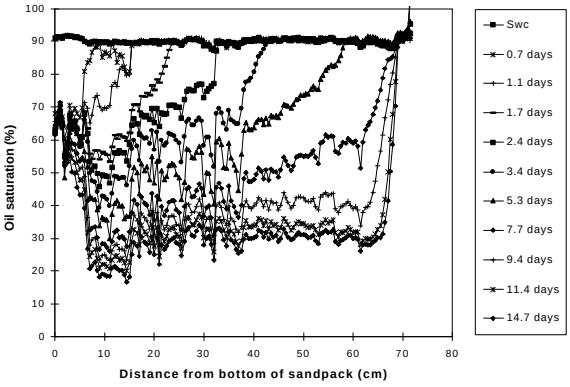

Figure 6: Oil Saturation Profiles for Waterflood of 21.7 cp Oil (Sandpack 3)

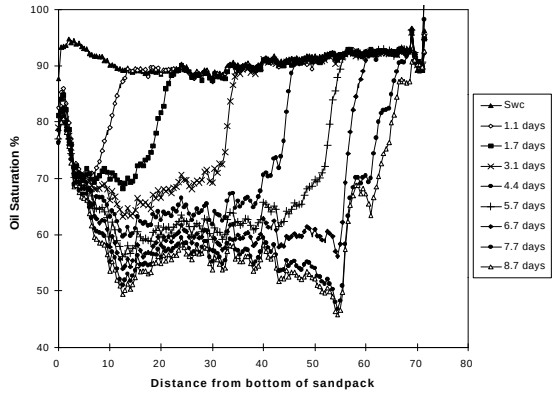

Figure 7: Oil Saturation Profiles for Waterflood of 210 cp Oil (Sandpack 1)

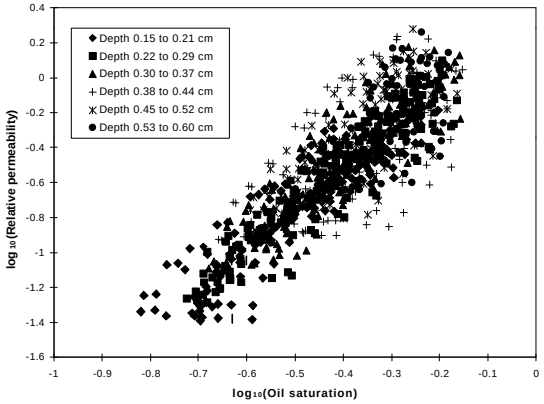

Figure 8: Oil Relative Permeabilities for Gas Gravity Drainage of 208 cp Oil (Sandpack 1)

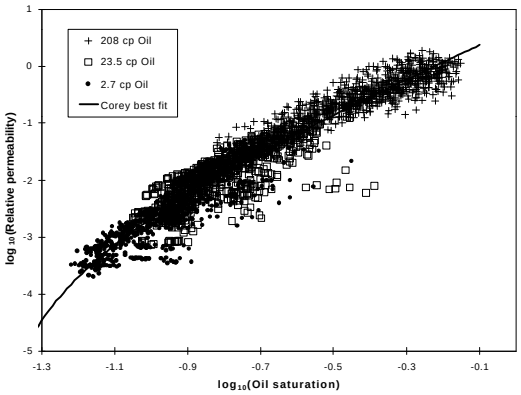

Figure 9: Comparison of Relative Permeabilities for Gas Gravity Drainage (Different Oil Viscosities)

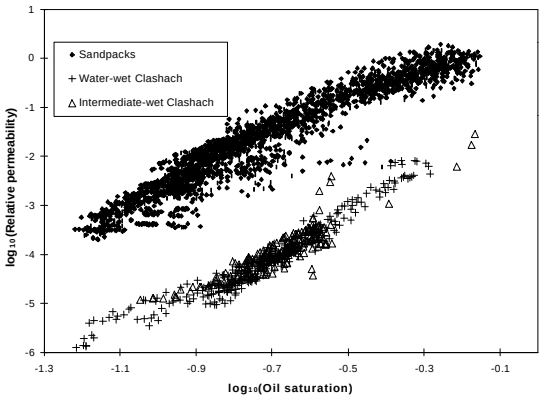

Figure 10: Comparison of Relative Permeabilities for Gas Gravity Drainage in Sandpacks and Clashach Sandstone

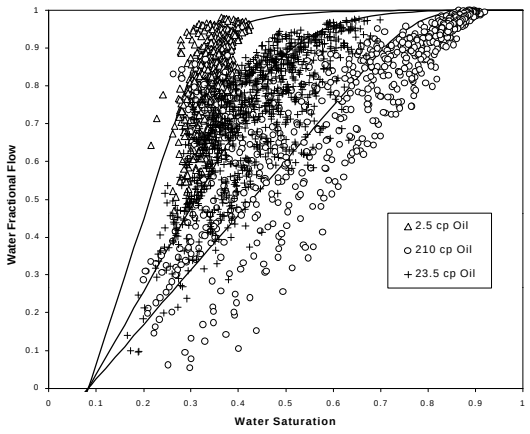

Figure 11: Water Fractional Flow Data from Three Waterflood Experiments

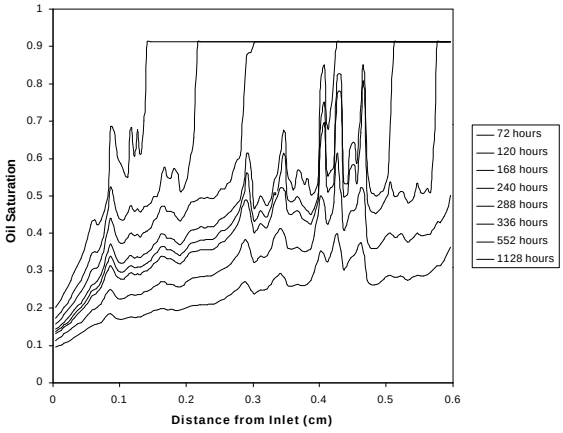

Figure 12: Simulated 208 cp Oil Saturation Profiles for Gas Gravity Drainage in Heterogeneous Pack with Capillary Pressure

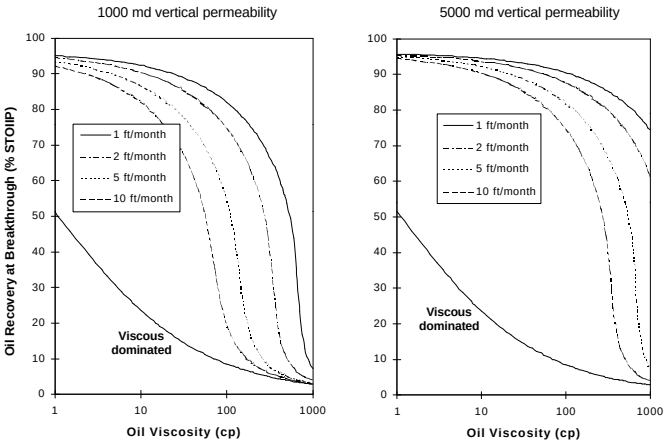

Figure 13: Oil Recovery Efficiency at Gas Breakthrough as a Function of Viscosity and Injection Rate

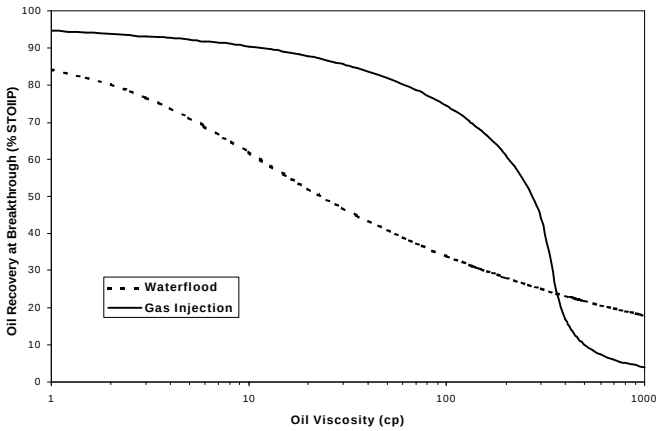

Figure 14: Oil Recovery at Breakthrough for Waterflood and Gas Injection (at 2 ft/month). Vertical Permeability 1 Darcy